www.czasopisma.pan.pl PAN www.journals.pan.pl
Chemical and Process Engineering 2021, 42 (3), 197–207
DOI: 10.24425/cpe.2021.138925

Analysis of liquid blending dynamics with Maxblend impellers by Electrical Resistance Tomography

Suzuka Iwasawa[1], Honami Kubo[1], Katsuhide Takenaka[1], Sandro Pintus[2], Francesco Maluta[3], Giuseppina Montante[3], Alessandro Paglianti[3]*

[1]Sumitomo Heavy Industries Process Equipment Co., Ltd. 1501, Imazaike, Saijo City, Ehime, Japan

[2]Retired from University of Pisa, Via Giunta Pisano 28, 56126 Pisa, Italy

[3]Department of Industrial Chemistry, University of Bologna, viale Risorgimento 4, 40136 Bologna, Italy

The aim of the investigation was liquid mixing time measurement in a laboratory scale stirred tank equipped with a metal Maxblend impeller and comparison with the corresponding mixing time obtained with other conventional impellers. The data are collected by Electrical Resistance Tomography, whose applicability in this case is non-trivial, because of the electrical interferences between the large paddles of the impeller and the measuring system. The raw data treatment methodology purposely developed for obtaining the homogenization dynamics curve is presented. A robust approach for a fine and low cost investigation of the mixing performances of close-clearance impellers in opaque systems is suggested. The analysis of the local and averaged conductivity time traces reveals the effect of important variables, such as the fluid viscosity and the vessel configuration, on the mixing time under various agitation conditions. The data collection and post processing procedures open the way to the application of the technique to multiphase and non-Newtonian fluids stirred with close-clearance impellers.

Keywords: Maxblend impeller, mixing time, Electrical Resistance Tomography, stirred tank

1. INTRODUCTION

Liquid mixing time is a frequently used parameter to compare mixing characteristics provided by different impellers. The advantages and limitations of the available experimental techniques for its determination, that include global and local methods, are generally well known (Jairamdas et al., 2019). One of the simplest local and non-intrusive techniques is based on Electrical Resistance Tomography (ERT) that is being increasingly adopted for the investigation of single-phase and multi-phase stirred tanks, as well as for a number of different operations of the chemical industry (Sharifi and Young, 2013). By the ERT technique, the time required to achieve homogenization of the liquid phase is estimated after the instantaneous injection of a concentrated aqueous salt solution in a less conductive medium. The measurement consists in detecting the time evolution of the local liquid conductivity or one of more measurement planes until the achievement of a constant conductivity value.

* Corresponding author, e-mail: alessandro.paglianti@unibo.it

This technique allows to investigate an opaque medium when the optical techniques cannot be used. Researchers mainly focused their attention on conventional fast impellers (e.g. Rushton turbines, Pitched Blade Turbine, Lightnin A310), whose diameter typically does not exceed half of the tank diameter. ERT has been also adopted with Maxblend impellers in case of shear-thinning fluid possessing yield stress (Patel et al., 2013) and solid liquid suspensions (Mishra and Ein-Mozaffari, 2016). Generally, the disturbance to the electric field due to the impeller is negligible, because of the sufficient distance from the electrodes. In addition, the physical variable fluctuations are not affected by the electric field variation due to the impeller rotation. The disturbance can also be smoothed if a large number of instantaneous samples is averaged, but the fast data rate, that is a typical advantage of ERT, must be renounced. Therefore, with close clearance impeller, the adoption of ERT at high data rate is a challenging task, because of the marked effects that large paddles induce on the electrical field in the measurement region. Among the close clearance impellers, the Maxblend impeller is selected, since its specific design is able to provide appropriate flow circulation and good performances in two-phase operations. It usually provides a good compromise between mixing efficiency and power consumption in a wide number of applications (Stobiac et al., 2014), its particular shape with paddle at the bottom surmounted by a grid proved to be very effective for generating efficient mixing at a low power consumption as compared with other impellers (Ameur, 2015). Overall, similarly to the case of static mixers (Montante et al., 2016), the flow features and the mixing mechanisms of the Maxblend impellers have been investigated in a relatively narrow number of works. The novel methodology presented in this work is expected to be of wide industrial interest considering the widespread adoption of large impellers for the mixing of opaque single phase and multiphase systems and the requirement of strict validation of modelling methods based on Computational Fluid Dynamics, that are widely adopted for the investigation of stirred tanks, including Maxblend impellers (e.g. Ameur et al., 2012).

In the following, a novel procedure purposely devised to extend the application of ERT to the case of large blade impellers is presented. The original data collected with the said methodology in single phase systems are discussed.

2. EXPERIMENTAL

The investigation was carried out in a cylindrical elliptical-bottom stirred tank of diameter $T = 232$ mm, either unbaffled or provided with four baffles of standard width ($W = T/10$). The elliptical bottom had a radius equal to 208 mm and a total volume of 1.6 L.

The vessel was filled with the liquid up to four different elevations equal to $H_{l,1} = 101$ mm, $H_{l,2} = 115$ mm, $H_{l,3} = 166$ mm $H_{l,4} = 231$ mm from the bottom of the cylindrical part of the vessel (z_0). Most of the experiments were performed with a Maxblend impeller type MB-S. For a comparative analysis the results obtained under the same conditions with a 6-bladed 45 ° Pitched Blade Turbine (PBT6) working in down-pumping mode were also considered. The schematic representation of the stirred tank equipped with the Maxblend impeller is depicted in Figure 1. The main geometrical characteristics of the impellers are summarized in Table 1.

As the working fluids, demineralized water and a solution of water and glycerol were adopted, resulting in viscosity in the range of $1–9 \cdot 10^{-3}$ Pa · s, for investigating the effect of the dynamic viscosity of the fluid on the mixing time. The impeller speed, N, was varied from 20 to 230 rpm. The impeller Reynolds numbers varied from a minimum value of about 800 with the water glycerol solution stirred with the Maxblend impeller to a maximum value of 60,000 obtained with water stirred with both the PBT and the Maxblend impeller.

Measurements were based on Electrical Resistance Tomography technique, by means of the ITS 2000 ERT instrumentation (Industrial Tomography Systems Ltd), that was already successfully adopted for the

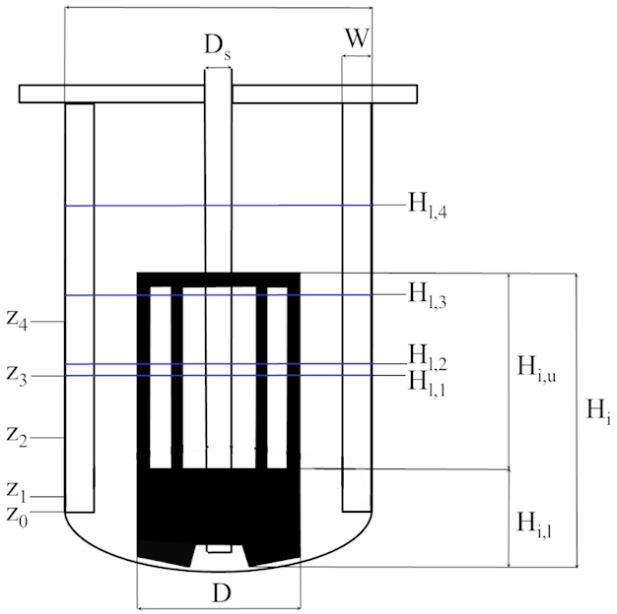

Fig. 1. Schematic representation of the stirred tank

Table 1. Main geometrical characteristics of the impellers and location of the measurement planes

Geometrical details	Size [mm]
Maxblend diameter, D	124
Maxblend height, H_i	223.6
Maxblend grid height $H_{i,u}$	149.2
Maxblend paddle height $H_{i,l}$	74.4
Maxblend clearance	4
PBT6 diameter, D	77
PBT6 clearance from z_0	77
Shaft diameter, D_s	18
Measuring plane 1, distance $z_0 - z_1$	12
Measuring plane 2, distance $z_0 - z_2$	57
Measuring plane 3, distance $z_0 - z_3$	102
Measuring plane 4, distance $z_0 - z_4$	147

mixing time measurements in single phase and two phase vessels stirred with fast impellers (e.g. Paglianti et al., 2017; Montante et al., 2019).

By the ERT instrumentation, electric current is injected from an adjacent electrode pair at a time and the voltage difference is measured from the remaining pairs of electrodes. The electrodes consisted of square stainless steel plates of the size of 20 × 20 mm. Four horizontal measurements planes with 16 electrodes per plane were adopted, fixed circumferentially on the vessel wall at the axial elevation reported in Table 1. The electrodes were then connected to the Data Acquisition System (DAS) by coaxial cables. In this work, the voltage difference was measured by the circular adjacent strategy (Dickin and Wang, 1996), the local

conductivity was obtained from the voltage measurements in real time by the linearized back projection algorithm similarly to previous investigations (e.g. Hosseini et al., 2010).

The amplitude and the frequency of the injected current were fixed at 15 mA and 9600 Hz respectively, after preliminary calibration tests. For each set of acquisitions, 500 total instantaneous measurements were collected, with an acquisition rate of 3.70 frames per second, thus closely following the dynamics of the process. For selected conditions, the measurements were repeated three times, obtaining a very good repeatability of the data. Other details on the technique can be found in previous investigations (Maluta et al., 2020).

3. ACQUISITION AND POST-PROCESSING OF THE RAW EXPERIMENTAL DATA

The local conductivity of the stirred liquid was measured by means of transient experiments, for obtaining the time evolution of the tracer homogenization on the four horizontal vessel sections equipped with the electrodes. A small amount of aqueous solution of sodium chloride (0.25 mL for 1 L of mixture) was rapidly injected at the top of the liquid free surface close to the wall. The measured variable was the raw dimensionless conductivity in the cell i, $C_i(t)$, that is the conductivity of the liquid at the generic time t, divided by the conductivity of the medium before the tracer injection, that was adopted as the so-called reference measurement. An example of the typical time trace of the dimensionless conductivity, $C(t)$, obtained from the average of the 316 local values on one measurement plane is shown in Figure 2. As a difference with the case of fast impellers, the experimental time trace obtained with the Maxblend shows a cyclic variation that is clearly related to the blade movements. Indeed, the data collected from 0 to 40 s were recorded before the injection of the concentrated salt solution, therefore the liquid conductivity variation cannot have arisen from any fluid dynamic effect.

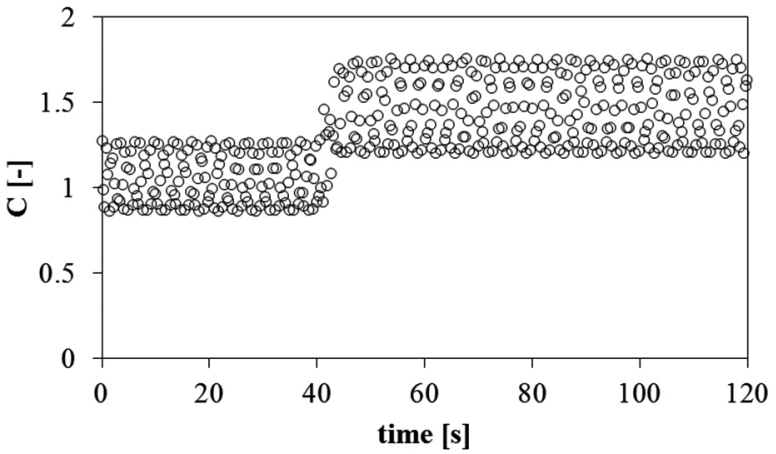

Fig. 2. Time trace of raw dimensionless conductivity; N = 75 rpm, $H_{l,4}$, water, baffled, z_1

In order to investigate the characteristic frequency of the signal oscillations, the frequency spectrum of the conductivity time trace was calculated. The spectral distribution of the conductivity was obtained by a standard spectral method implemented in the MatLab® software, namely the Fast Fourier Transform (FFT), that is appropriate being the ERT samples collected at equidistant times. The typical frequency resolution of the spectral distribution was equal to 0.0145 Hz. The result for the time trace reported in Figure 2 is shown in Figure 3.

The peak in Figure 3 clearly shows that the periodicity of the conductivity corresponds to the impeller rotation frequency, that is equal to 1.25 rps. Therefore, the filtration of the impeller frequency was

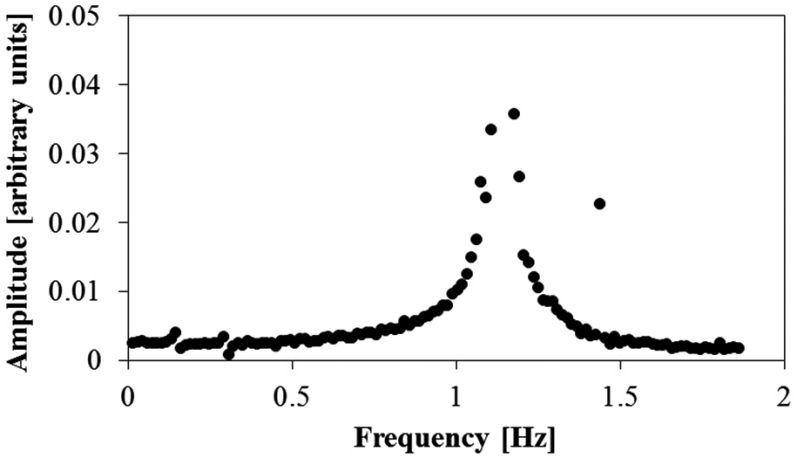

Fig. 3. Frequency spectrum of the dimensionless conductivity time trace shown in Figure 2

performed by subtracting a sinusoidal signal of frequency equal to that identified by the FFT analysis to the conductivity time trace for removing the strong effect of the electrical interference between the electrodes and the impeller. The filtered signal is shown in Figure 4.

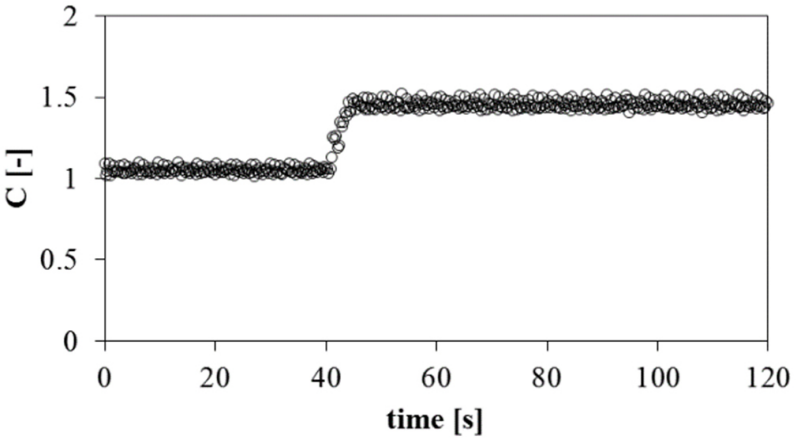

Fig. 4. Dimensionless filtered conductivity time trace shown in Figure 2

The comparison between the experimental data shown in Figure 2 and in Figure 4 clearly indicates that for measuring the mixing time with ERT in the case of large blade impellers, the raw signal has to be filtered by removing the electrical noise due to the impeller passage.

In addition to the filtering procedure, in order to directly compare the results of subsequent runs, removing the effect of the initial and final conductivity values, the local dimensionless conductivity is further normalized, resulting in the following normalized local conductivity, $\chi_i(t)$:

$$\chi_i(t) = \frac{C_i(t) - C_i(t_{in\,j})}{C_i(t_\infty) - C_i(t_{in\,j})} \tag{1}$$

where $C_i(t_{in\,j})$ is the conductivity measured before the tracer addition and $C_i(t_\infty)$ is the value obtained at the complete homogenization, therefore, $\chi_i(t_{in\,j}) = 0$ and $\chi_i(t_\infty) = 1$, irrespective of the initial and final conductivity values. The liquid mixing time is defined as the time required to reach a level of variation within $\pm(1 - x)\%$ of $\chi_i(\infty)$, being x the desired degree of homogeneity.

The final form of the time trace adopted for the analysis of the results, after filtering, normalization, averaging on the measurement plane of the raw data, is shown in Figure 5.

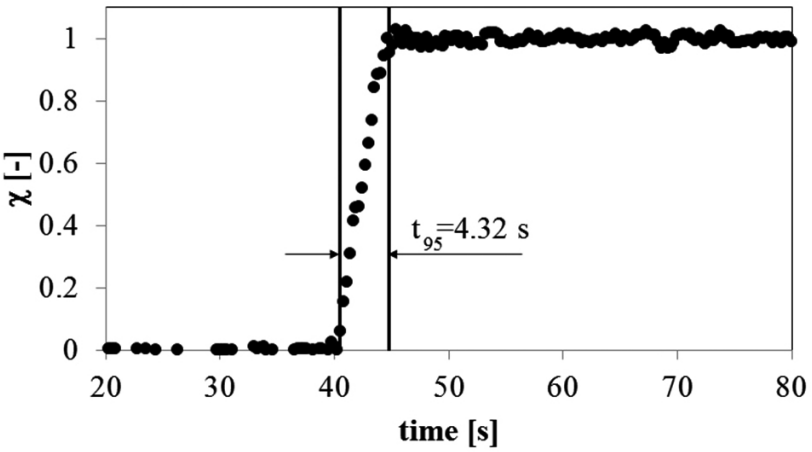

Fig. 5. Normalized conductivity time trace; N = 75 rpm $H_{l,4}$, water, baffled, z_1

In the following, the mixing time is evaluated as the time corresponding to the 95% homogeneity level, t_{95}, that, for the case shown in Figure 5, corresponds to 4.32 s.

The robustness of the data post-processing procedure has been checked, not only on the mean conductivity values, but also on the local values. In Figure 6, the local unfiltered conductivity tomograms before the injection of the conductive tracer are shown.

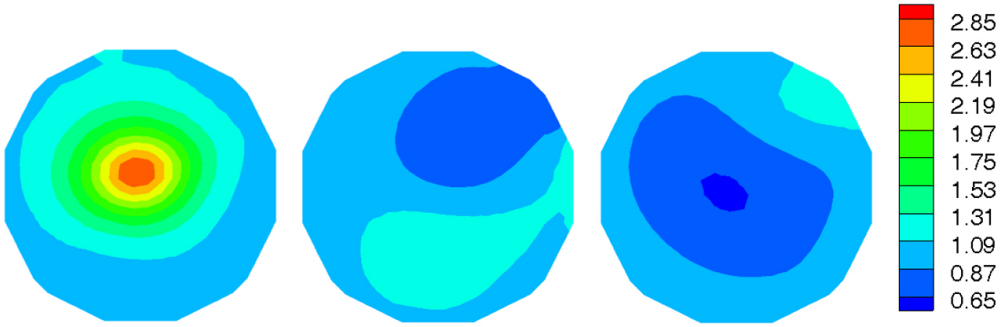

(a) (b) (c)

Fig. 6. Tomograms of instantaneous local dimensionless conductivity on z_1, raw data. N = 75 rpm, (a) t = 20.25 s, (b) t = 20.79 s, (c) t = 21.06 s

As already observed for the plane averaged curves, the large local conductivity variations clearly reveal the effect of the movement of the metallic impeller on the ERT data.

Figure 7 allows to appreciate the effect of the filtering procedure on the data plotted in Figure 6.

As can be observed, the effect of the impeller passage is removed. Nevertheless, for all the snapshots the local conductivity value is greater in the centre, due to the effect of the impeller position on the acquisition used as a reference. For removing also this minor non-fluid dynamic effect, it is sufficient to use the normalized conductivity, instead of the dimensionless values, as shown in Figure 8, where just a negligible deviation from homogeneity is observed.

Finally, based on the observation above, the following procedure is suggested for obtaining reliable experimental ERT data for the characterization of close clearance impellers in stirred tanks:

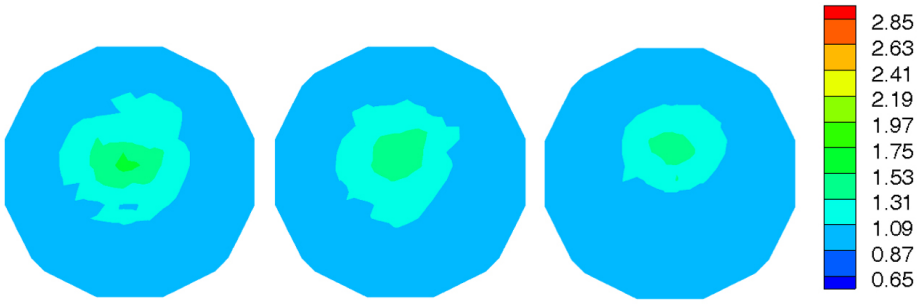

Fig. 7. Tomograms of instantaneous filtered local dimensionless conductivity shown in Figure 6, (a) t = 20.25 s, (b) t = 20.79 s, (c) t = 21.06 s

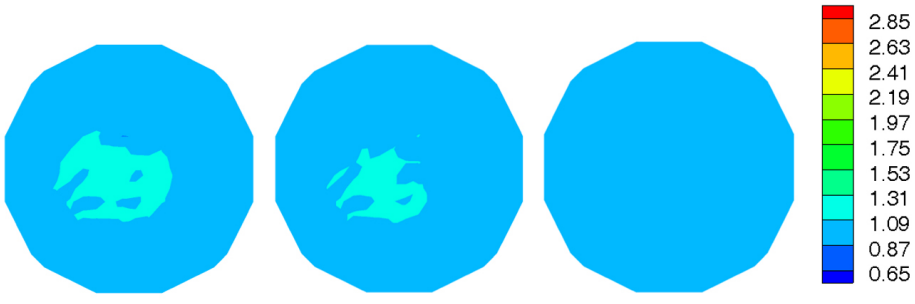

Fig. 8. Tomograms of instantaneous filtered and normalized local conductivity shown in Figure 6; (a) t = 20.25 s, (b) t = 20.79 s, (c) t = 21.06 s

- Measurement of the liquid conductivity during the tracer homogenization, adopting a reference measurement in the stirred liquid before the tracer addition, for obtaining the dimensionless conductivity map over time, $C_i(t)$.
- FFT analysis of the dimensionless conductivity time trace and identification of the characteristic signal frequency by reading the peak on the frequency spectrum.
- Filtering raw data for removing the periodic effect due to the impeller passage.
- Normalization of the filtered signal by Eq. (1), for obtaining the normalized dimensionless conductivity over time, $\chi_i(t)$.

The results collected with this procedure are discussed in the following section.

A preliminary evaluation of the mixing time obtained in this way by comparison with the value computed with the well-known correlation of Grenville and Nienow (2004) provides a satisfactory result, since the dimensionless mixing time, $N \cdot t_{95}$, measured with water in our baffled vessel stirred with the PBT is equal to 44 and the value obtained with the correlation adopting a power number of 1.7 is equal to 40.

4. RESULTS AND DISCUSSION

An example of the acquisitions on four measuring planes is reported in Figure 9. The analysis of the normalized conductivity time evolution shows that, right after the injection at the free liquid layer, the concentrated solution moves towards the centre of the tank and vertically downward, due to both its momentum and the impeller action.

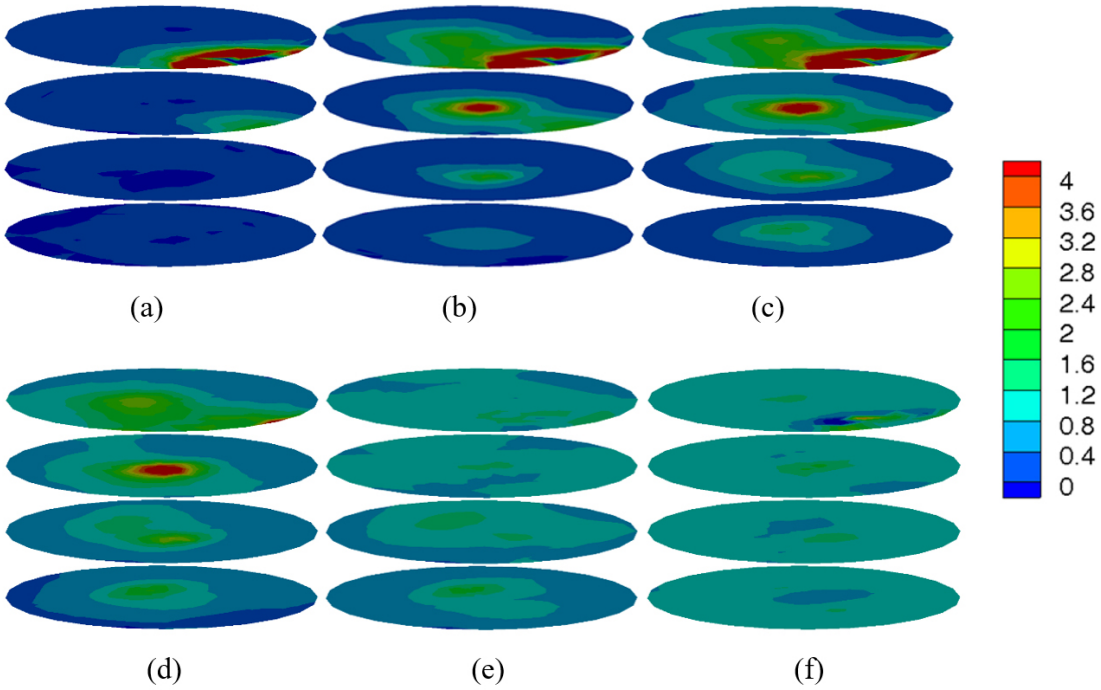

Fig. 9. Tomograms of instantaneous local normalized conductivity on the four measurement planes (z_1, z_2, z_3, z_4 from bottom to top), MB-S impeller, N = 100 rpm, (a) t = 40 s, (b) t = 41 s, (c) t = 42 s, (d) t = 43 s, (e) t = 44 s, (f) t = 45 s

Its dispersion towards the bottom of the tank occurs mainly in the centre of the tank, suggesting that the impeller induces an axial movement that is directed downwards in the centre of the tank and upwards close to the tank wall. Injecting at the top of the vessel, the last measuring plane reaching the homogenization is the closest to the vessel bottom.

In the following, the analysis of the mixing time estimated from the mean normalized conductivity time traces, $\chi(t)$ measured on the z_1 plane, that is the farthest from the injection point, as a function of the working conditions (impeller speed, presence/absence of baffles, liquid height and liquid viscosity) will be performed.

The experimental data shown in Figure 10 confirm that, as expected, the impeller speed has a strong influence on the mixing time, while the liquid level and the viscosity of the liquid phase have a weaker

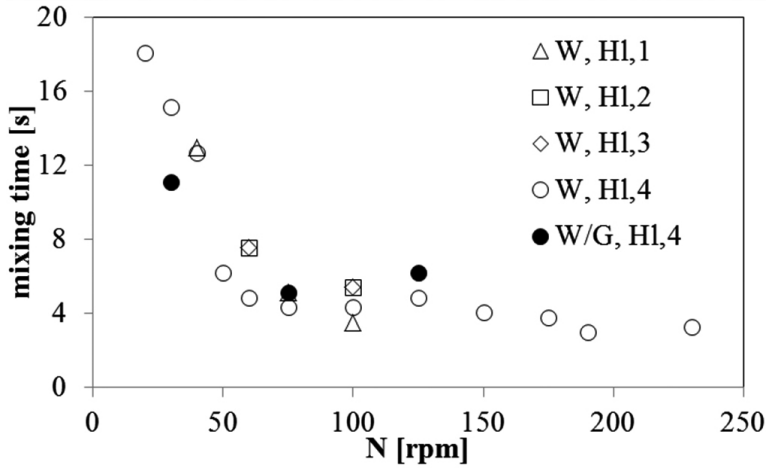

Fig. 10. Effect of liquid level ($H_{l,i}$) and liquid type (W – water; W/G – water/glycerol solution) on mixing time, baffled stirred tank

effect. It is worthwhile noticing that the dynamic viscosity was changed only by a factor of 10 and both the tested liquid phases exhibited a Newtonian behavior. A more important effect was noticed after removing the baffles from the vessel, as shown in Figure 11. The qualitative trend of the mixing time is similar to that presented by Fradette et al. (2007).

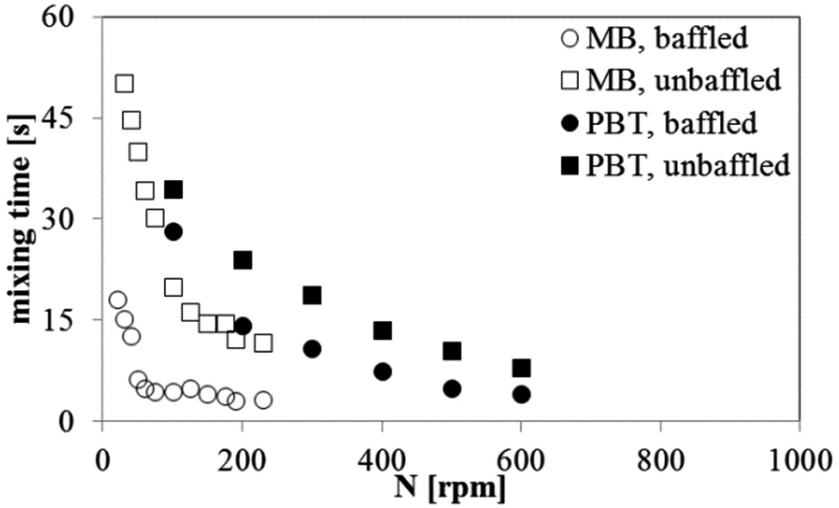

Fig. 11. Comparison between mixing time in the baffled and unbaffled stirred vessel stirred with Maxblend (MB) and PBT

The comparison between present and literature experimental data is not straightforward, because of the geometrical differences between the Maxblend impellers adopted in different investigations. The main difference is that the diameter of the Maxblend adopted in the present investigation was constant along the vertical axis, in fact the top and the bottom impeller diameters are equal, while previous investigations were carried out with impellers characterized by a diameter that was larger at the bottom and smaller at the top with the ratio between the top and the bottom impeller diameter of about 0.73. The other important difference is in the gap between the impeller and the baffles. In fact the D/T ratio in this work was equal to 0.53, Fradette et al. (2007) adopted different impellers with D/T in the range of 0.72–0.75, Guntzburger et al. (2013) had an impeller with $D/T = 0.72$. Table 2 shows the comparison between the asymptotic value of the dimensionless mixing time, that in present work was obtained with water only, and that in the previous investigations.

Table 2. Dimensionless mixing time in baffled tanks stirred with Maxblend impellers

Authors	Liquid phase	$N \times t_{95}$
Present work	Water	10.2
Fradette et al. (2007)	Newtonian and non-Newtonian fluids	10–11
Guntzburger et al. (2013)	glucose and glycerol aqueous solution	≈ 3

In Figure 11 the comparison between the mixing time measured in the tank stirred with the Maxblend and the PBT is also reported. The mixing time obtained with the Maxblend is generally lower than that measured with the PBT, both in baffled and in unbaffled configuration. Comparison at equal power consumption will be also performed after collecting power consumption curves.

5. CONCLUSIONS

The investigation presented in this work leads to the identification of a robust procedure for the collection, post-processing and analysis of ERT data in tanks stirred with close-clearance impellers. The procedure ensures to avoid limitations due to the possible effect of the movement of large impeller blades close to the electrodes on the measured conductivity. The methodology was applied to the determination of the mixing time obtained with a Maxblend impeller in a baffled and unbaffled tank in single phase flow. Due to the wide application of large blade impellers in the industrial mixing of opaque non-Newtonian fluids and dense multiphase systems, the methodology described in this work is expected to be widely useful for the investigation of the mixing characteristics in a broad range of applications and scales.

SYMBOLS

a	exponent
$C(t)$	plane-average of $C_i(t)$
$C_i(t)$	local instantaneous dimensionless conductivity in the i-th cell at t
D	impeller diameter, mm
H_i	Maxblend impeller height, mm
$H_{l,1-4}$	liquid heights, mm
N	impeller rotational speed, rpm
T	Tank diameter, mm
t	time, s
t_{95}	mixing time to achieve a 95% degree of homogeneity, s
W	baffle width, mm
x	degree of homogeneity
z_0	axial coordinate of the bottom of the cylindrical part of the vessel, mm
z_{1-4}	axial coordinate of the measuring planes, mm

Greek symbols

$\chi(t)$	plane-average of $\chi_i(t)$
$\chi_i(t)$	normalized local instantaneous dimensionless conductivity in the i-th cell at t

Subscripts

i	cell of the tomogram

REFERENCES

Ameur H., 2015. Energy efficiency of different impellers in stirred tank reactors. *Energy*, 93, 1980–1988. DOI: 10.1016/j.energy.2015.10.084.

Ameur H., Bouzit M., Helmaoui M., 2012. Hydrodynamic study involving a maxblend impeller with yield stress fluids. *J. Mech. Sci. Technol.*, 26, 1523–1530. DOI: 10.1007/s12206-012-0337-3.

Dickin F., Wang M., 1996. Electrical resistance tomography for process applications. *Meas. Sci. Technol.*, 7, 247–260. DOI: 10.1088/0957-0233/7/3/005.

Fradette L., Thomé G., Tanguy P.A., Takenaka K., 2007. Power and mixing time study involving a Maxblend® impeller with viscous Newtonian and non-Newtonian fluids. *Chem. Eng. Res. Des.*, 85, 1514–1523. DOI: 10.1205/cherd07051.

Grenville R.K., Nienow A.W., 2004. Blending of miscible liquids, In: Paul E.L., Atiemo-Obeng V.A., Kresta S.M. (Eds.). *Handbook of industrial Mixing: Science and practice*. John Wiley & Sons, Inc. Chapter 9, 507–542. DOI: 10.1002/0471451452.ch9.

Guntzburger Y., Fontaine A., Fradette L., Bertrand F., 2013. An experimental method to evaluate global pumping in a mixing system: Application to the Maxblend™ for Newtonian and non-Newtonian fluids. *Chem. Eng. J.*, 214, 394–406. DOI: 10.1016/j.cej.2012.10.041.

Hosseini S., Patel D., Ein-Mozaffari F., Mehrvar M., 2010. Study of solid-liquid mixing in agitated tanks through electrical resistance tomography. *Chem. Eng. Sci.*, 65, 1374–1384. DOI: 10.1016/j.ces.2009.10.007.

Jairamdas K., Bhalerao A., Machado M.B., Kresta S.M., 2019. Blend time measurement in the confined impeller stirred tank. *Chem. Eng. Technol.*, 42, 1594–1601. DOI: 10.1002/ceat.201800752.

Maluta F., Montante G., Paglianti A., 2020. Analysis of immiscible liquid-liquid mixing in stirred tanks by Electrical Resistance Tomography. *Chem. Eng. Sci.*, 227, 115898. DOI: 10.1016/j.ces.2020.115898.

Mishra P., Ein-Mozaffari F., 2016. Using tomograms to assess the local solid concentrations in a slurry reactor equipped with a Maxblend impeller. *Powder Technol.*, 301, 701–712. DOI: 10.1016/j.powtec.2016.07.007.

Montante G., Carletti C., Maluta F., Paglianti A., 2019. Solid dissolution and liquid mixing in turbulent stirred tanks. *Chem. Eng. Technol.*, 42 (8), 1627–1634. DOI: 10.1002/ceat.201800726.

Montante G., Coroneo M., Paglianti A., 2016. Blending of miscible liquids with different densities and viscosities in static mixers. *Chem. Eng. Sci.*, 141, 250–260. DOI: 10.1016/j.ces.2015.11.009.

Paglianti A., Carletti C., Montante G., 2017. Liquid mixing time in dense solid-liquid stirred tanks. *Chem. Eng. Technol.*, 40, 862–869. DOI: 10.1002/ceat.201600595.

Patel D., Ein-Mozaffari F., Mehrvar M., 2013. Using tomography to characterize the mixing of non-Newtonian fluids with a Maxblend impeller. *Chem. Eng. Technol.*, 36, 687–695. DOI: 10.1002/ceat.201200425.

Sharifi M., Young B., 2013. Electrical Resistance Tomography (ERT) applications to Chemical Engineering. *Chem. Eng. Res. Des.*, 91, 1625–1645. DOI: 10.1016/j.cherd.2013.05.026.

Stobiac V., Fradette L., Tanguy P.A., Bertrand F., 2014. Pumping characterisation of the maxblend impeller for Newtonian and strongly non-Newtonian fluids. *Can. J. Chem. Eng.*, 92, 729–741. DOI: 10.1002/cjce.21906.

Received 17 June 2021
Received in revised form 12 August 2021
Accepted 24 August 2021